Electrostatic Ion Cyclotron and Ion Plasma Waves in a Symmetric Pair-Ion Plasma Cylinder

M. Kono,[1,*] J. Vranjes,[2] and N. Batool[3]
[1]Faculty of Policy Studies, Chuo University, Tokyo 192-0393, Japan
[2]Institute of Physics Belgrade, Pregrevica 118, 11080 Zemun, Serbia
[3]National Center of Physics, Islamabad 44000, Pakistan

(Received 28 February 2013; revised manuscript received 21 October 2013; published 12 March 2014)

Complicated wave behavior observed in the cylindrical pair-ion (fullerene) experiments by Oohara and co-workers are now identified to be low harmonic ion cyclotron waves combined with ion plasma oscillations inherent to kinetic theory. The electrostatic dispersion equation derived is based on an approximation for the current from the exact solutions of the characteristic cylindrical geometry form of the Vlasov plasma equation in a uniform magnetized plasma cylinder surrounded by a larger metal boundary outside a vacuum gap, which thus differs from that in unbounded plasmas. Positive and negative ions, differing only in the sign of their charge, respond to a potential in the same time scale and cooperate to reflect the enhanced kinetic orbital behaviors to the macroscopic propagation characteristics. In addition, the experimental value of the Larmor radius (comparable to the discharge radius but small enough to make the analytic approximation useful) makes higher harmonic ion cyclotron effects both observable and calculable with the appropriate approximation for the kinetic theory.

DOI: 10.1103/PhysRevLett.112.105001 PACS numbers: 52.30.Ex, 52.27.Cm, 52.27.Ep, 52.35.Fp

After the pioneering experimental studies on propagation properties of electrostatic waves in symmetric pair-ion plasmas [1–5] (singly charged positive and negative fullerene ions), there have appeared a number of theoretical works on various linear and nonlinear modes in pair-ion plasmas [6–17]. However, basic propagation characteristics observed in the experiments have not been adequately explained yet. This is because those works are based on fluid theories of unbounded plasmas in spite of kinetic natures seen in the experimental data. One sees several separated solutions, each extending over a frequency range $m\Omega$ to $(m \pm 2)\Omega$ (with the exception of a low-frequency branch going from 0 to Ω), all of which indicates the strong effect of kinetic cyclotron resonances. The significance of pair-ion plasmas is that it is produced in laboratories and provides new insights into phenomena in pair plasmas in general. This holds both in the laboratory environment (due to clear advantages of being free from the usual problem of annihilation inherent to antimatter electron-positron plasma), and under astrophysical environments with similar pair (electron-positron) plasmas where antimatter plasma is frequently found. A main feature of pair-ion plasmas is that positive and negative ions respond to a potential in the same time scale and expose the kinetic orbital effects to the level of the macroscopic properties like propagation characteristics. In this Letter, we develop a kinetic theory in a cylindrical coordinate system to treat whole eigenmodes in a unified manner. Exact solutions of the characteristic equations of the linearized Vlasov equation lead to an approximate kinetic dispersion equation. The dispersion relations of the low and high frequency backward waves and some forward waves are terminated at certain wave numbers k_z due to the fact that the local solutions of dispersion equation then become complex if k_z is increased and not due to the cyclotron damping. In a cylindrical system, the cyclotron resonance damping is not effective since particles are unlikely to come back to the same phase of the wave after one cyclotron period. The essential feature of the results presented here is that standard classic kinetic theory is still enough to explain the puzzling experimental results that remained elusive in spite of many attempts, yet stressing that pair-ion plasma is a new kind.

For a plasma confined in a cylindrical vessel immersed in a constant magnetic field $\mathbf{B}$ in the axial z direction, we solve the Vlasov equation in cylindrical coordinates

$$\frac{\partial}{\partial t}F_\alpha + \left(v_r\frac{\partial}{\partial r} + \frac{v_\theta}{r}\frac{\partial}{\partial \theta} + v_z\frac{\partial}{\partial z}\right)F_\alpha + \left[\left(\Omega_\alpha v_\theta + \frac{v_\theta^2}{r}\right)\frac{\partial}{\partial v_r} - \left(\Omega_\alpha v_r + \frac{v_r v_\theta}{r}\right)\frac{\partial}{\partial v_\theta}\right]F_\alpha = \frac{e_\alpha}{m_\alpha}\left(\frac{\partial \phi}{\partial r}\frac{\partial}{\partial v_r} + \frac{1}{r}\frac{\partial \phi}{\partial \theta}\frac{\partial}{\partial v_\theta} + \frac{\partial \phi}{\partial z}\frac{\partial}{\partial v_z}\right)F_\alpha, \quad (1)$$

where $\Omega_\alpha = e_\alpha B/m_\alpha c$ and α denotes the species as $\alpha = \pm$, and the continuity and the Poisson equations

$$\nabla \cdot \left\{\frac{\partial \mathbf{E}(\mathbf{r},t)}{\partial t} + \sum_\alpha 4\pi n_{0\alpha} e_\alpha \int \mathbf{v} F_\alpha(\mathbf{r},\mathbf{v},t)d\mathbf{v}\right\} = 0. \quad (2)$$

The equilibrium is $F_{\alpha 0}(\mathbf{v}) = F_{\alpha 0}(v_\perp, v_z)$, $v_\perp^2 = v_r^2 + v_\theta^2$, and we choose $F_{\alpha 0}$ to be Maxwellian. Now we introduce a

fluctuation f_α through $F_\alpha(\mathbf{r},\mathbf{v},t)=F_{\alpha 0}(v_\perp,v_z)+f_\alpha(\mathbf{r},\mathbf{v},t)$, and linearize Eq. (1) to get

$$\frac{df_\alpha}{dt}=\frac{e_\alpha}{m_\alpha}\left(\frac{\partial\phi}{\partial r}\frac{\partial}{\partial v_r}+\frac{1}{r}\frac{\partial\phi}{\partial\theta}\frac{\partial}{\partial v_\theta}+\frac{\partial\phi}{\partial z}\frac{\partial}{\partial v_z}\right)F_{\alpha 0}, \tag{3}$$

where d/dt is the total derivative. Equation (3) is integrated along the characteristic orbit in the phase space which is defined by $dr/dt=v_r$, $d\theta/dt=v_\theta/r$, $dz/dt=v_z$, $dv_z/dt=0$, $dv_r/dt=v_\theta^2/r+\Omega_\alpha v_\theta$, and $dv_\theta/dt=-v_\theta v_r/r-\Omega_\alpha v_r$. Since we have three invariants, $E=v_r^2+v_\theta^2=v_\perp^2$, $L=v_\theta r+(\Omega_\alpha/2)r^2$, and v_z, we may introduce a variable $\varphi(t)$ through $v_r=v_\perp\cos\varphi$ and $v_\theta=v_\perp\sin\varphi$. Equations for $\varphi(t)$ and $\theta(t)$ then reduce to $d\varphi/dt=-(v_\perp/r)\sin\varphi-\Omega_\alpha$, $d\theta/dt=-d\varphi/dt-\Omega_\alpha$, where $r(t)=r_L[-\varepsilon\sin\varphi(t)+(\sin^2\varphi(t)+2\kappa)^{1/2}]$ is derived from the invariant $L(\kappa=L\Omega_\alpha/v_\perp^2)$ and r_L is the Larmor radius defined by $r_L=v_\perp/|\Omega_\alpha|$ and $\varepsilon=|\Omega_\alpha|/\Omega_\alpha$. Since $r(t)$ is non-negative, $\kappa\geq 0$. The $\varphi(t)$ and $\theta(t)$ are

$$\begin{aligned}\varphi(t)&=\tilde{\varphi}_0-\Omega_\alpha t-\varepsilon\sin^{-1}[\cos\varphi(t)/s(\kappa)]\\&=\Phi(t)-\sin^{-1}\frac{\cos\Phi(t)}{\sqrt{2[1+\kappa+\varepsilon s(\kappa)\sin\Phi(t)]}},\end{aligned} \tag{4}$$

$$\theta(t)=\tilde{\theta}_0+\varepsilon\sin^{-1}[\cos\varphi(t)/s(\kappa)], \tag{5}$$

where $\Phi(t)=\tilde{\varphi}_0-\Omega_\alpha t$, $s(\kappa)=\sqrt{1+2\kappa}$, $\varphi_0=\varphi(0)$, $\tilde{\varphi}_0=\varphi_0+\sin^{-1}[\cos(\varphi_0/s(\kappa))]$, $\theta_0=\theta(0)$, and $\tilde{\theta}_0=\theta_0-(\tilde{\varphi}_0-\varphi_0)$. The $z(t)$ and $r(t)$ are integrated as $z(t)=v_z t+z_0$,

$$\begin{aligned}r(t)&=r_L\sqrt{2[1+\kappa+\varepsilon s(\kappa)\sin\Phi(t)]}+\tilde{r}_0\\&=r_L p(\kappa)\sin\psi(t)+\tilde{r}_0,\end{aligned} \tag{6}$$

where $\psi(t)=\cos^{-1}[q(\kappa)\cos(\Phi(t)/2+\varepsilon\pi/4)]$, $p(\kappa)=\sqrt{2[1+\kappa+s(\kappa)]}$, $q(\kappa)=2s(\kappa)/p(\kappa)$, $r_0=r(0)$, $\tilde{r}_0=r_0-r_L\sqrt{1+\kappa+\varepsilon s(\kappa)\sin\tilde{\varphi}_0}$ and $z_0=z(0)$.

Since the exact solutions in Eqs. (5) and (6) are unfortunately not directly applicable to integrating Eq. (3) along the orbit (as was the case for Cartesian geometry) we now use the following approximation. Noting $s(\kappa)\geq 1$ and $|\cos\varphi/s(k)|\leq 1$, $\theta(t)$ is approximated as $\theta(t)\simeq\tilde{\theta}_0+\varepsilon S(\kappa)\cos\Phi(t)$, where $S(\kappa)=\sin^{-1}[1/s(\kappa)]$. In a similar way using the conditions $q(\kappa)\leq 1$ and $|q(\kappa)\cos\psi(t)|\leq 1$ in Eq. (6), we may approximate $\psi(t)$ as $\psi(t)\simeq\pi/2+Q(\kappa)\cos[\Phi(t)/2+\varepsilon\pi/4]$, where $Q(\kappa)=\sin^{-1}q(\kappa)$, leading to

$$\begin{aligned}r(t)&=r_L p(\kappa)\sin\psi(t)\simeq r_L p(\kappa)\cos\{Q(\kappa)\cos[\Phi(t)/2\\&\quad+\varepsilon\pi/4]\}\\&=r_L p(\kappa)\{J_0[Q(\kappa)]+2\sum_{n\geq 1}J_{2n}[Q(\kappa)]\cos[n(\Phi(t)\\&\quad+\varepsilon\pi/2)]\}.\end{aligned} \tag{7}$$

Here, J_ℓ is the Bessel function of the first kind and positive definite since $Q(\kappa)$ is smaller than the first zero of J_0. In the following we retain only J_0 and J_2 since J_{2n} with $n>2$ is negligible compared with J_0 and J_2.

Now (r',θ') at t' are represented by (r,θ) at t as $r'=r+2r_L p(\kappa)J_2(Q(\kappa))[\sin(\Omega_\alpha\tau+\varphi)-\sin\varphi]$, $\theta'=\theta+\xi(\tau)$, where $\tau=t'-t$, $\xi(\tau)=-\Omega_\alpha\tau/2+\tan^{-1}[g(\tau)]-\tan^{-1}[g(0)]$, and $g(\tau)=[(1+\kappa)\tan(\Omega_\alpha\tau/2+\theta)+s(\kappa)]/\kappa$. The usual convenient assumption in kinetic theory of uniform density $n_{\alpha 0}$ is also made here so that the calculation of the plasma current can go forward; in the end the justification for this is whether the result is in acceptable agreement with experiment. Introducing the Fourier-Hankel transform $\phi(r,\theta,z,t)=\sum_{\mathbf{k}}\sum_\ell\phi_\ell(k_\perp,k_z,\omega)J_\ell(k_\perp r)\exp[i\ell(\theta+\pi/2)+i(k_z z-\omega t)]$ where $\mathbf{k}_\perp=(k_\perp\cos\rho,k_\perp\sin\rho)$, Eq. (3) is expressed as

$$\begin{aligned}f_\ell(r,k_z,\mathbf{v},\omega)=\frac{n_{\alpha 0}e_\alpha}{m_\alpha}\sum_{k_\perp}\phi_\ell(k_\perp,k_z,\omega)\Bigg\{&J_\ell(k_\perp r)e^{i\ell\pi/2}\frac{1}{v_\perp}\frac{\partial F_{\alpha 0}}{\partial v_\perp}+i\left(\frac{\omega-k_z v_z}{v_\perp}\frac{\partial F_{\alpha 0}}{\partial v_\perp}+k_z\frac{\partial F_{\alpha 0}}{\partial v_z}\right)\sum_m J_m(k_\perp r)\\&\times\sum_{m_1}\cdots\sum_{m_4}J_{m_1}(\beta)\cdots J_{m_4}(\beta)\delta(\ell-[m+m_1-m_2-m_3+m_4])e^{im\pi/2}e^{i(m_1+m_2-m_3-m_4)\varphi}\\&\times\int_{-\infty}^{0}d\tau e^{-i(\omega-k_z v_z-(m_1+m_2)\Omega_\alpha)\tau-i\ell\xi(\tau)}\Bigg\},\end{aligned} \tag{8}$$

where $\beta=k_\perp r_L p(\kappa)J_2(Q(\kappa))\simeq k_\perp r_L/2$. In the following we only consider the case of $\ell=0$ since the oscillation potential observed in the experiment is maximum at the center. Then $\xi(\tau)$ no longer has a contribution in the integration over the time and it may be neglected in Eq. (8). Next, the current estimated through $\mathbf{j}_\ell(r,k_z,\omega)=\sum_\alpha e_\alpha\int\mathbf{v}f_{\alpha\ell}(r,k_z,\mathbf{v},\omega)d\mathbf{v}$ is substituted into Eq. (2) to give the electric displacement as

$$\mathbf{D}=\begin{pmatrix}K_\perp & iK_{\perp 2} & 0\\ -iK_{\perp 2} & K_\perp & 0\\ 0 & 0 & K_z\end{pmatrix}\begin{pmatrix}E_r\\E_\theta\\E_z\end{pmatrix}, \tag{9}$$

where for the Maxwellian $F_{\alpha 0}$,

$$K_\perp = 1 + \sum_\alpha \frac{1}{k_\perp^2 \lambda_\alpha^2} \sum_m d_m(\eta) \frac{2m\Omega_\alpha}{k_z v_T} \frac{W(\zeta_{2m+1}) + W(\zeta_{2m-1})}{2},$$

$$K_{\perp 2} = \sum_\alpha \frac{\Omega_\alpha}{k_\perp v_{T\alpha}} \frac{\omega_\alpha^2}{\Omega_\alpha^2} \sum_m [I'_m(\eta) - I_m(\eta)] \times \frac{W(\zeta_{2m+1}) - W(\zeta_{2m-1})}{2},$$

$$K_z = 1 + \sum_\alpha \frac{1}{k_z^2 \lambda_\alpha^2} \left[1 + \sum_m d_m(\eta) \zeta_{2m} W(\zeta_{2m}) \right],$$

$d_m(\eta) = I_m(\eta) e^{-\eta}$, $\eta = k_\perp^2 r_L^2/4$, $W(\zeta)$ is the plasma dispersion function defined by $W(\zeta) = (1/\sqrt{2\pi}) \int_C [1/(x-\zeta)] \exp(-x^2/2) dx$, $\zeta_{2m} = (\omega - 2m\Omega_\alpha)/(k_z v_{T\alpha})$, and we have used $\int_0^\infty u J_n(\alpha u) J_n(\beta u) e^{-u^2} du = (1/2) I_n(\alpha\beta/2) e^{-(\alpha^2+\beta^2)/4}$, $\sum_n J_n(\eta)^2 = 1$, $\sum_n I_n(\eta) e^{-\eta} = 1$. Now Eq. (2) (i.e., the Poisson equation) reads

$$K_\perp \left\{ \frac{1}{r} \frac{\partial}{\partial r} \left[r \frac{\partial}{\partial r} J_\ell(k_\perp r) \right] - \frac{\ell^2}{r^2} J_\ell(k_\perp r) \right\} - k_z^2 K_z J_\ell(k_\perp r) = 0,$$

where $k_\perp$ is determined by

$$k_\perp^2 K_\perp + k_z^2 K_z = 0. \tag{10}$$

The dispersion relation is determined by the boundary condition. Since the plasma is detached from the wall, the boundary conditions are that the normal displacement and tangential electric fields are continuous at the plasma boundary, yielding

$$K_\perp k_\perp \frac{J'_\ell(k_\perp r_*)}{J_\ell(k_\perp r_*)} - \frac{\ell}{r_*} K_{\perp 2} = k_z \frac{\phi'_{\rm out}(k_z r_*)}{\phi_{\rm out}(k_z r_*)}, \tag{11}$$

for which we put $\ell = 0$. Outside the plasma the potential is a solution of the Laplace equation $\nabla^2 \phi_{\rm out} = 0$ with the condition $\phi_{\rm out}(R) = 0$ at the wall $r = R$, that is $\phi_{\rm out}(k_z r) = A[K_0(k_z R) I_0(k_z r) - I_0(k_z R) K_0(k_z r)]$, where K_0 and I_0 are the modified Bessel functions. Thus, the waves are determined by solving Eqs. (10) and (11) for which the plasma is assumed to be $\Omega_+ = \Omega_- = \Omega$, $v_{T+} = v_{T-} = v_T$, $\omega_+^2 = \omega_-^2 = \omega_p^2$, and the ion Debye lengths $\lambda_+^2 = \lambda_-^2 = \lambda^2 = v_T^2/\omega_p^2$.

The parameters used here are the same as those in the experiment, the density $n_0 = 1 \times 10^8$ cm^{-3} of the fullerene plasma with $m_i = 720 m_p$ ($\omega_p/2\pi = 78.2$ kHz), the magnetic field $B = 0.2$ T ($\Omega/2\pi = 4.2$ kHz), the temperature $T_+ = T_- = 0.3$ eV (in the experiment $T_+ \sim T_- \sim$ 0.3–0.5 eV), the plasma radius $r_* = 1.5$ cm, and the vessel radius $R = 4$ cm, respectively. Thus, $\lambda = 0.04$ cm, $r_L = 0.75$ cm, and $v_T = 200$ m/s.

Dispersion equations.—For the plasma satisfying the inequality $\omega_p > \Omega > k_z v_T$, we may rely on the asymptotic expansion of the plasma dispersion function in Eqs. (10) and (11), and we obtain

$$1 = \frac{2}{k^2 \lambda^2} \sum_{m=-\infty}^{\infty} d_m \{ C_0(m,x) + C_1(m,x) \}, \tag{12}$$

$$1 - G(k_\perp, k_z) = \frac{2}{k_\perp^2 \lambda^2} \sum_{m=-\infty}^{\infty} d_m C_1(m,x), \tag{13}$$

where $k^2 = k_\perp^2 + k_z^2$, $x = \omega/\Omega$, $C_1(m,x) = 2m(2m+1)/[x^2 - (2m+1)^2] + 6m(2m+1) k_z^2 r_L^2/[x^2 - (2m+1)^2]^2$, $C_0(m,x) = k_z^2 r_L^2/[x^2 - (2m)^2] + 2(2m)^2 k_z^2 r_L^2/[x^2 - (2m)^2]^2$, and $G(k_\perp, k_z) = (k_z/k_\perp)(\phi'_{\rm out}(k_z r_*)/\phi_{\rm out}(k_z r_*)) \times (J_0(k_\perp r_*)/J'_0(k_\perp r_*))$. Equations (12) and (13) give an alternative dispersion equation

$$\frac{1}{2} [k_z^2 + k_\perp^2 G(k_\perp, k_z)] \lambda^2 = \sum_{m=-\infty}^{\infty} d_m C_0(m,x). \tag{14}$$

In the following we solve Eqs. (13) or (14) to get $\omega = \omega(k_\perp, k_z)$ and substitute the result into Eq. (12) to get the relation between k_z and $k_\perp$ numerically. The coefficient $d_m(\eta)$ is rapidly decreasing with m and increasing with η, the higher order resonances become effective for larger η. The reason we retain up to the second order expansion of the plasma dispersion function is because it plays a definite role in the vicinity of the resonance. In the experiment the Larmor radius is comparable to the half of the vessel radius, implying the waves of higher m are excitable.

The novel cylindrical analysis developed here, especially in its various approximations, proves to agree remarkably well with the experimental results. This can be more clearly seen when one develops these approximations in detail, the topic to which we now turn.

Wave solutions under various approximations.—In the experiment, two branches of backward waves exist in the low and intermediate frequency ranges although the low-frequency backward wave is clearly observed only when waves are excited by a grid exciter.

Low-frequency waves $\omega < \Omega$: Eq. (16): Since the backward wave in $0 < \omega < \Omega$ is supposed to be a coupled mode of the thermal and ion cyclotron modes, we eliminate $k_\perp^2$ from Eqs. (12) and (13) and retain terms with resonances in this frequency range to obtain

$$d_0 \frac{k_z^2 r_L^2}{x^2} - \hat{G} d_1 \left[\frac{2}{x^2 - 1} + \frac{6 k_z^2 r_L^2}{(x^2-1)^2} \right] - \frac{k_z^2 \lambda^2}{2} = 0, \tag{15}$$

where $\hat{G} = G/(1-G)$. As is expected when the parallel wave number is small, so the $k_z^2 \lambda^2$ term in Eq. (15) can be dropped, yielding

$$\omega^2 = (b_1 \Omega^2/b_2) \{ 1 \pm \sqrt{1 - d_0 k_z^2 r_L^2 b_2/b_1^2} \}, \tag{16}$$

where $b_1 = d_0 k_z^2 r_L^2 - \hat{G} d_1 (1 - 3k_z^2 r_L^2)$ and $b_2 = d_0 k_z^2 r_L^2 - 2\hat{G} d_1$. This is substituted into Eq. (12) to fix the relation between $k_\perp$ and k_z. The solution, Eq. (16), is depicted by the purple curves in Fig. 1: the solutions with + and − signs are backward and forward, respectively. In Fig. 1 the dots are experimental data given in Fig. 6 of [4]: the blue dots are for the waves excited by a cylindrical exciter and the red ones are by a grid exciter. Since the difference is observed only for the low-frequency waves, the experimental data by the grid exciter are plotted only for the low-frequency backward and forward waves. The solution, Eq. (16), fits the data by the cylindrical exciter for the parameters mentioned above. The dispersion curves are terminated at $k_z/2\pi \sim 0.05$ where the solution, Eq. (16), becomes complex. The $k_\perp$ is almost constant around $k_\perp r_* \sim 1.035$ and less than the first zero of the eigenfunction $J_0(k_\perp r)$. The data by the grid exciter are reproduced by the same solution, Eq. (16), but now with $T = 0.1$ eV and $k_\perp r_* \sim 2.653$ which is between the first and the second zeros of the eigenfunction. For both cases $G(k_\perp, k_z) > 0$, implying the low-frequency backward and forward waves do not induce surface charges.

Intermediate frequency backward wave $2\Omega < \omega < 4\Omega$: Eq. (18): These waves are regarded to be from single dispersion curve. However, based on our dispersion equations [(13) and (14)], the experimental data are supposed to consist of two branches, one from Eq. (14) and the other from Eq. (13). First we consider Eq. (14), which is written as

$$\frac{1}{2}[k_z^2 + k_\perp^2 G]\lambda^2 = \sum_{m\neq\pm 2} d_m C_0(m,x) + \frac{64 d_2 k_z^2 r_L^2}{(x^2-16)^2}. \quad (17)$$

The solution of Eq. (17) is approximated by

$$\frac{\omega^2}{\Omega^2} = 16 - \left\{ \frac{64 d_2 k_z^2 r_L^2}{(k_z^2 + k_\perp^2 G)\lambda^2/2 - b_3} \right\}^{1/2}, \quad (18)$$

where $b_3 = \sum_{m\neq\pm 2} d_m C_0(m,4)$. Equation (18) is substituted into Eq. (12) to get the sets of $k_\perp$ and k_z. The solution, Eq. (18), is depicted in Fig. 1 by a brown curve. In the experiment, the long wave part of the dispersion relation is not observed, while Eq. (18), unlike Eq. (16), does not provide an upper limit on k_z (usually a "nose" in an ω vs k_z plot), beyond which the frequency values are complex. It might be due to the rough approximation used above. The $k_\perp r_*$ value is around 3.863 between the first and second zeros of the eigenfunction and $G(k_\perp, k_z) > 0$.

Intermediate frequency $3\Omega < \omega < 5\Omega$: Eq. (20): In the frequency range $3\Omega < \omega < 5\Omega$, Eq. (13) reads

$$(1-G)\frac{k_\perp^2\lambda^2}{2} = \sum_{m\neq -3,2} d_m C_1(m,x) + \frac{60 d_2 k_z^2 r_L^2}{(x^2-25)^2}, \quad (19)$$

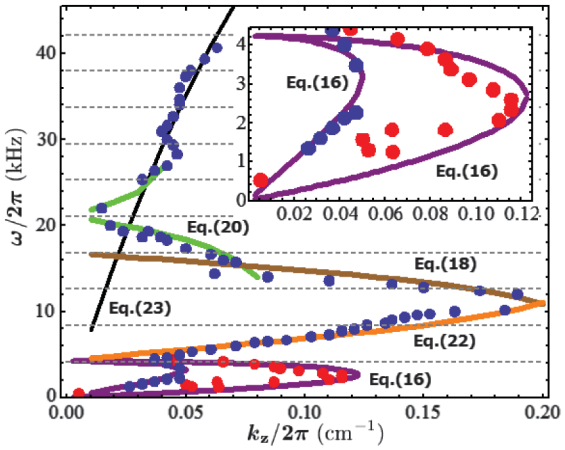

FIG. 1. (color) The dispersion relations of the axially propagating waves of $\ell = 0$. The details are in the text. The enlarged figure of the dispersion relations of the low-frequency backward or forward waves is embedded. The labels on the theory curves give the equation number and the horizontal dotted lines indicate the cyclotron resonance frequencies $\omega/2\pi = m\Omega/2\pi$, $m = 1, 2, \ldots$.

and the solution is approximately given by

$$\frac{\omega^2}{\Omega^2} = 25 \pm \left\{ \frac{60 d_2 k_z^2 r_L^2}{(1-G)k_\perp^2\lambda^2/2 - b_4} \right\}^{1/2}, \quad (20)$$

where $b_4 = \sum_{m\neq -3,2} d_m C_1(m,5)$. The solution, Eq. (20), with the − sign, is depicted in Fig. 1 by a green curve. The dispersion relation of this wave is terminated at the wave number at $k_z/2\pi = 0.08$ for the backward wave beyond which $G(k_\perp, k_z) \geq 1$ so that $1 - G$ becomes negative and ω becomes complex. The $k_\perp r_*$ value is around 1.452 for which b_4 is neglected; that is, the effects of the remote resonances are neglected. For large $k_\perp$, b_4 is not neglected and the similar solution is obtained when $k_\perp r_* \sim 7.275$ for which the eigenfunction has two nodes. This is because $G(k_\perp, k_z)$ has to be negative and the real solution of Eq. (20) exists only for large values of $k_\perp r_*$.

A fragment of the forward wave dispersion relation around $\omega/2\pi \sim 5\Omega$ is given by the solution Eq. (20) with the + sign and is shown in green in Fig 1. The branch is terminated at $k_z/2\pi = 0.04$ and $k_\perp r_* \sim 1.313$.

Ion cyclotron wave: The frequency range is $\Omega < \omega < 3\Omega$, for which we solve Eq. (13):

$$(1-G)\frac{k_\perp^2\lambda^2}{2} = \sum_{m\neq 0,1} d_m C_1(m,x) + \frac{6 d_1 k_z^2 r_L^2}{(x^2-1)^2}, \quad (21)$$

where the term $2d_1/(x^2-1)$ is neglected since this term is dominated over by the second term of the right-hand side. The solution is given by

$$\frac{\omega^2}{\Omega^2} = 1 + \left\{ \frac{6 d_1 k_z^2 r_L^2}{(1-G) k_\perp^2 \lambda^2 / 2 - b_5} \right\}^{1/2}, \tag{22}$$

where $b_5 = \sum_{m \neq 0,1} d_m C_1(m, 1)$. The solution is depicted in Fig. 1 by an orange curve. The $k_\perp r_*$ is 0.39 and $G(k_\perp, k_z) > 0$.

High frequency wave: In the high frequency range $\omega \gg \Omega$, Eq. (13) gives $G(k_\perp, k_z) = 1$ which determines the relation between $k_\perp$ and k_z. Then we solve Eq. (14) in which we keep only the term of $m = 0$ to give

$$\omega^2 = 2 d_0 \frac{k_z^2}{k_\perp^2 + k_z^2} \omega_p^2. \tag{23}$$

This is the ion plasma wave in a cylindrical system and depicted in Fig. 1 by a black curve. Certainly $k_\perp r_*$ is less than the first zero of the eigenfunction. Note that in Ref. [4] the density estimated from the dispersion relation $\omega = \sqrt{2}\omega_p$ is 3.3×10^6 although the value measured by the probe is 1×10^8. This discrepancy is resolved by using our derived expression which fits the experimental data with $n = 1 \times 10^8$.

High frequency cyclotron waves: In the frequency range $\omega > 5\Omega$, Eq. (13) does not give real solutions for the ion cyclotron harmonic waves. However, in the experiment there is a tiny fragment of the dispersion curve of the backward wave at $\omega \sim 7\Omega$. Appropriate approximations to display these features have yet to be found.

Summary.—We have analyzed the propagation characteristics of electrostatic waves in a homogeneous pair-ion plasma in a cylindrical system and shown based on a kinetic theory that the observed waves are identified to be ion cyclotron harmonic waves in the intermediate frequency range and a coupled wave of ion cyclotron mode and ion thermal mode in the low-frequency range. The noticeable Larmor radius is crucial for higher harmonic cyclotron resonances to play definite roles in the dispersion equations and makes the first few harmonic ion cyclotron waves observable. Thus, in order to explain experiments, a kinetic theory is needed together with cyclotron and cylindrical effects. However, the story may still be one sided and incomplete, because the same may hold for trapping which cannot be ruled out [18,19], and a complete picture can only be delivered by treating all these aspects simultaneously.

One of the authors (M. K.) would like to thank Professor H. Saleem for fruitful discussions. This work was supported by a Grant-in-Aid for Science Research from the Ministry of Education, Culture, Sports, Science, and Technology, Japan.

*kono@fps.chuo-u.ac.jp

[1] W. Oohara and R. Hatakeyama, Phys. Rev. Lett. **91**, 205005 (2003).
[2] W. Oohara, D. Date, and R. Hatakeyama, Phys. Rev. Lett. **95**, 175003 (2005).
[3] W. Oohara and R. Hatakeyama, Phys. Plasmas **14**, 055704 (2007).
[4] W. Oohara, Y. Kuwabara, and R. Hatakeyama, Phys. Rev. E **75**, 056403 (2007).
[5] W. Oohara, T. Hibino, T. Higuchi, and T. Ohta, Rev. Sci. Instrum. **83**, 083509 (2012).
[6] J. Vranjes and S. Poedts, Plasma Sources Sci. Technol. **14**, 485 (2005).
[7] H. Schamel and A. Luque, New J. Phys. **7**, 69 (2005).
[8] F. Verheest and T. Cattaert, Phys. Plasmas **12**, 032304 (2005).
[9] H. Saleem, J. Vranjes, and S. Poedts, Phys. Lett. A **350**, 375 (2006).
[10] F. Verheest, Phys. Plasmas **13**, 082301 (2006).
[11] B. Zhao and J. Zheng, Phys. Plasmas **14**, 062106 (2007).
[12] J. Vranjes, D. Petrovic, B. P. Pandey, and S. Poedts, Phys. Plasmas **15**, 072104 (2008).
[13] J. Vranjes and S. Poedts, Phys. Plasmas **15**, 044501 (2008).
[14] H. Schamel, Phys. Plasmas **16**, 113709 (2009).
[15] F. Anderegg, C. F. Driscoll, D. H. Dubin, T. M. O'Neil, and F. Valentini, Phys. Plasmas **16**, 055705 (2009).
[16] H. Saleem, N. Batool, and S. Poedts, Phys. Plasmas **18**, 052108 (2011).
[17] F. Verheest, M. A. Hellberg, and W. A. Hereman, Phys. Plasmas **19**, 092302 (2012).
[18] H. Schamel, Phys. Plasmas **19**, 020501 (2012).
[19] H. Schamel, Phys. Plasmas **20**, 034701 (2013).